J. Applied Membrane Science & Technology, Vol. 24, No. 3, December 2020, 99–120

High-Performance Nanosilver Thin Film Nanocomposite Membranes Prepared on Carbon Nanotube-Based Supports

N. N. Gumbi[a]*, B. S. Mbuli[b], M. O. Daramola[c], S. D. Mhlanga[d], B. B. Mamba[a], E. N. Nxumalo[a]

[a]Institute for Nanotechnology and Water Sustainability, College of Science, Engineering, and Technology, University of South Africa, Florida ,1709 Johannesburg, South Africa
[b]Department of Chemical Sciences, University of Johannesburg, P.O. Box 17011, Doornfontein 2028, South Africa
[c]Department of Chemical Engineering, Faculty of Engineering, Built Environment and Information Technology, University of Pretoria, Private Bag X20 Hatfield, Pretoria, 0028, South Africa
[d]DST/MINTEK Nanotechnology Innovation Centre and SabiNano Pty Ltd, Mintek, 200 Malibongwe Drive, Strijdom Park, Randburg, 2194, Johannesburg, South Africa

Submitted: 21/10/2020. Revised edition: 16/11/2020. Accepted: 16/11/2020. Available online: 19/11/2020

ABSTRACT

Biofouling in membranes is a serious concern as it leads to a severe reduction in membrane performance by increasing the membranes' resistance to permeate flow. This work describes a facile method for the production of high performance nanosilver polyamide thin-film nanocomposite (TFN) membranes on carbon nanotube-based supports for biofouling control. The TFN membranes were prepared by the interfacial polymerization of a thin polyamide layer over a polyethersulfone (PES) support layer. Nanosilver (nAg) particles were generated in-situ on the surface of the polyamide layer using a reduction reaction between a silver salt and sodium borohydride. The support layer of the TFN membrane contained nitrogen doped multi-walled carbon nanotubes (N-MWCNTs) at various dosages. The SEM/EDS microscopic analyses revealed that nAg particles were present on the polyamide layer and that they were evenly distributed throughout the TFN membrane. Furthermore, the TFN membrane showed an improved water permeability (from 16.74 L/m^2.h to 22.86 L/m^2.h at 150 Psi) without sever compromise in NaCl rejection (from 98.37% to 99.40%) compared to the bare TFC membrane. This was attributable to the combined hydrophilic effects imparted by the presence of nAg on the TFN polyamide layer and the oxidised CNTs in the support layer. Antibacterial tests conducted using *Escherichia coli* bacteria demonstrated that the TFN containing nAg particles membranes exude better antibacterial activity compared to the pristine TFC membrane as evidenced by a clear zone of inhibition, in the area surrounding the TFN membrane and the absence of bacterial colonies. The present study demonstrated that the presence of low dosages of CNTs in the support layer is essential in the improvement of mechanical strength and performance properties of the support layer, while nAg plays a crucial role in the enhancement of TFN membrane performance.

Keywords: Thin-film nanocomposites, nanosilver, carbon nanotubes, nitrogen-doped carbon nanotubes, biofouling

* Corresponding to: N. N. Gumbi (email: gumbinn@unisa.ac.za)
DOI: https://doi.org/10.11113/amst.v24n3.201

1.0 INTRODUCTION

Recent developments in water treatment research have been focused towards the exploitation of desalination technology for the treatment of sea and brackish water to obtain safe and potable water. This approach holds a promising future for increasing freshwater supply. Among others, thin-film composite (TFC) membranes are commonly employed in the reverse osmosis (RO) process for water desalination. In TFC membranes, each individual layer can be optimized individually in order to obtain a composite membrane with desirable properties [1]. However, despite their elegant design, TFC membranes are largely polymer-based and are therefore prone to membrane fouling, particularly biofouling. Biofouling, which is caused by growth of biofilm on the membrane surface in TFC membranes, is of serious concern since it hinders the performance of the membrane thus limiting the membranes' prolonged use. Biological foulants such as bacteria, fungi and algae grow in large quantities on the membrane surface thereby inhibiting permeation through the membrane surface [2]. The use of strong oxidizing agents such chlorine, ozone, etc., to remove the adsorbed biofilm may be detrimental to the membrane's structure as they are capable of degrading the polyamide layer on TFC membranes [3, 4].

Silver and silver-containing compounds are well-known for their biocidal properties. Moreover, the advent of nanotechnology has enabled further engineering of these silver-containing compounds to generate nanomaterials that possess much enhanced antibacterial activity and other remarkable features owing to their nanoscale dimensions. Particularly, silver nanoparticles or nanosilver particles (nAg) has found wide-spread use as fillers for membrane modifications to reduce membrane biofouling. The proposed mechanisms of the nAg antibacterial activity include (i) uptake of free Ag+ ions, (ii) the disruption of ATP production and DNA replication, (iii) nAg and silver ion generation of the reactive oxygen species, and (iv) direct damage of the cell membranes by nAg [5].

Direct addition of nAg into the feed water stream to inactivate bacteria would require massive amounts to be added and would therefore be very expensive [6]. Hence, immobilizing small amounts of nAg on the membrane surface where biofilm growth takes place is a more plausible approach. The use of nAg in membranes has been intensively studied on polyethersulfone (PES) and polysulfone (PSf) mixed-matrix membranes [7-13]. Relevant literature reports in which nAg has been used for TFC membrane modification is summarized in Table 1. In most cases, the membrane performance in terms of flux and rejection was negatively affected by the incorporation of nAg.

A study by Kim and co-workers, investigated the effects of incorporation of nAg and CNTs into the polyamide layer and PSf support layer [14]. Their findings revealed that anti-biofouling, permeability and solute rejection properties of the resultant TFN membrane were greatly improved upon the inclusion of nAg and CNTs. Previously, Phao et al., prepared PES UF membranes modified with low dosages of nitrogen-doped carbon nanotubes (N-CNTs) and reported that the fabricated membranes exhibited enhanced water permeabilities and mechanical strength properties due to the high surface reactivity of the N-CNTs [15]. Therefore, the present study aims to

systematically investigate the role of oxidized multi-walled carbon nanotubes (O-MWCNTs) or nitrogen-doped multi-walled carbon nanotubes (N-MWCNTs) in PES-based supports for the fabrication of high performance TFN membranes. Moreover, in-situ generation of nAg on the polyamide layer was conducted to enhance evaluate the anti-biofouling properties of the TFN membrane. The TFC and TFN membranes fabricated were studied using a range of spectroscopic and microscopic techniques and their performance was evaluated using the cross-flow filtration system.

Table 1 Nanosilver incorporated TFC membranes with their corresponding membrane performance

Nanosilver loading method	**nAg/TFC membrane performance**	**Reference**
nAg particles were dispersed in the organic phase (in HCFC) during TFC membrane formation.	-Membranes' water flux and salt rejection were maintained. -*Pseudomonas spp* were destroyed on contact with membrane surface. -Most of the nAg remained intact after filtration tests.	[16]
In-situ generated on TFC surface: reduction reaction between AgNO3 and FCOH.	-Slower decrease in permeate flux and TDS rejection. -Microbial cell growth on membrane surface was prevented.	[17]
nAg were dispersed in the aqueous phase (with MPD) during TFC membrane formation.	-Increase in hydrophilicity and water permeability. -Antifouling and antibacterial activity was displayed against *Pseudomonas aeruginosa.*	[14]
In-situ generated on TFC surface: reduction reaction between $AgNO_3$ and $NaBH_4$	-Strong antibacterial activity (75% of live bacteria removed). -Biofilm formation was suppressed. -Surface and transport properties of the membrane were retained.	[6]

*FCOH= Formaldehyde *HCFC= 1, 1 Dichloro-1-flueroethane

2.0 EXPERIMENTAL

2.1 Materials

Toluene (99.8%), ferrocene (98.0%), acetonitrile (99.8%) and N-methyl-2-pyrrolidinone (NMP) (99.5%) were all purchased from Sigma-Aldrich South Africa. CNTs and N-CNTs were freshly prepared in our laboratory using a conventional catalytic chemical vapour deposition (CCVD) method. Nitric acid (HNO_3) used for the MWCNT purification and functionalisation was purchased from Merck South Africa. Polyethersulfone (Veradel 3000P) was supplied by Solvay Advanced Polymers (South Africa). Deionized (DI) water was obtained from a water purification system (RO Process Ecopure G.I.C. Scientific). The 1,3-phenylenediamine (MPD) ≥ 99%, 1,3,5-benzenetricarbonyl

trichloride (TMC) >98%, n-hexane (95%), sodium dodecyl sulphate (99%), sodium borohydride (≥ 99%), silver nitrate and sodium carbonate were all purchased from Sigma-Aldrich South Africa. Silver nitrate (99.0%) was purchased from Merck South Africa.

2.2 Preparation of CNT/PES and N-CNT/PES Support Membrane

The CNT/PES and N-CNT/PES blend membranes were prepared using the non-solvent induced phase inversion method [18]. Firstly, weighed amounts of oxidised CNTs or N-CNTs (0.1 and 1.0 wt.%) were dispersed in NMP solvent by ultrasonication for 10 min to increase dipersibility, followed by the addition of 15wt% PES to form CNT/PES and N-CNT/PES blends. The casting solutions were allowed to stir at 80 °C for 2 h for complete dissolution of the polymer and efficient mixing with additives. The casting solution were left to settle overnight at room temperature for degassing. The solutions were then cast onto the glass plate using a casting knife (Elcometer 3545 Adjustable Bird Film Applicator) at a set thickness of 200 µm. The coated glass plate was allowed to air dry for 10 s followed by immersion in a non-solvent water bath at 4 °C for 2 h. The resultant membrane was rinsed with deionised water at room temperature, dried and stored between sheets of paper.

2.3 Preparation of TFC and TFN RO Membranes

Thin-film composite (TFC) membranes were prepared via interfacial polymerisation method [19], where in 0.1wt% O-MWCNT/PES and N-MWCNT/PES blend supports were first, pre-treated in sodium dodecyl sulphate (0.5 wt.%) solution for 12 h. The membranes were then rinsed with deionised water and allowed to air dry. The support membranes were then taped onto a glass plate around the edges and immersed in a 2.0 wt.% m-phenylene diamine (MPD) aqueous solution (previously adjusted to pH= 8 with ammonium chloride) for 3 min. The excess MPD solution on the taped membrane substrate was removed with a rubber roller, followed by soaking in a 0.1 wt.% trimesoyl chloride (TMC) in n-hexane solution for about 1 min for interfacial polymerisation to take place. After 1 min of reaction, the glass plate was held vertically to remove excess TMC solution followed by curing in the oven at 65 °C for 15 min. The resultant TFC membranes were washed with a 0.2 wt.% Na_2CO_3 solution and deionised water to remove any unreacted monomers.

To prepare TFN membranes, the TFC membrane was taped on a glass plate and immersed in $AgNO_3$ solution for 5 min. The excess $AgNO_3$ solution was removed leaving only a thin residual layer. The glass plate was then immersed in $NaBH_4$ solution for 2 min to allow the reduction of Ag^+ ions into Ag^0 on the TFC membrane surface. The membranes were then rinsed with deionized water at room temperature. The concentrations of $AgNO_3$ and $NaBH_4$ solutions were varied from 0.005 M - 0.25 M. The results reported in this study are however based on the 0.25 M:0.25 M ($AgNO_3$:$NaBH_4$) solution as no Ag could be detected on the TFC membrane surface at low molar concentration ratio (0.005 M:0.005 M and 0.1 M:0.1 M). Membranes denoted as “TFC” in study, were not coated with nAg on the polyamide layer, while membranes denoted as “TFN” were coated with nAg.

2.4 Characterization of TFC and TFN Membranes

Surface morphology of membranes was characterised by a VEGA3 TESCAN

Scanning Electron Microscope (SEM) under a 20 kV electron acceleration voltage. Membrane samples were sputter-coated with gold before analysis to prevent charging. Information on surface roughness of the membranes was obtained from Dimension 3100 Veeco atomic force microscopy (AFM) in tapping mode using the camera model Nanoscope III. Fourier transformed (FT-IR) spectra were collected from a Fourier transformed infrared spectrometer (Perkin-Elmer Spectrum) equipped with attenuated total reflectance (ATR) accessory.

Surface crystalline properties of membranes were studied using a X Pert Diffractometer by PAnalytical. X-ray diffraction spectra were collected at a scan range between 3 - 90º, by exposing samples to X-rays at an applied voltage and current of 40 kV and 30 mA using Cu K-beta radiation= 1.454 Å. The instrument was equipped with scintillation counter detector. Thermogravimetric analysis (TGA) of the samples was carried out by using a Perkin-Elmer TGA 4000 analyser, in which 8 mg of the sample was heated in a temperature range of 30 - 900°C at a heating rate of 10°C/min in oxygen atmosphere at a flow rate of 20 ml/min. Data Physics Optical Contact Angle analyser using a sessile drop method was used to evaluate the membranes hydrophilicity. An average of 10 contact angle readings was taken from different locations on each membrane type.

Mechanical strength properties of PES blended, TFC, nad TFN membraes assess the impact of CNT (or N-CNT) incorporation on the PES composite membranes' mechanical performance, 3 - 4 equal sized specimens (9 cm length, 1 cm width) of each sample underwent tensile tests at a force of 2 N. The stress-strain curve for the polymeric membranes was obtained by applying a tensile force at a uniform speed of 1 mm/min. The measurements were taken from an electronic stretching machine (AG-IC SHIMADZU control/measuring unit) at a strain rate of 1 mm/min.

2.5 Membrane Performance Tests

Transport properties of membranes were examined using the cross-flow filtration system (Sterlitech, USA) with a membrane cell area of 42 cm^2. In the case of support membrane performance, the membranes were firsts compacted for 1 h at 150 Psi, following which, the applied pressure was varied between 50 – 150 Psi to evaluate membrane permeability. For TFC membrane performance evaluation, the membranes were compacted for 6 h at 300 Psi (20.7 bar, followed by varying the applied pressure between 100 to 300 Psi. The pure water flux of membranes was calculated using Equation (1) as:

$$J_{w1} = \frac{V}{A \times t} \tag{1}$$

Where V is the permeate volume (L), A is the membrane effective area (cm^2) and t is the time (h) necessary for the permeate volume to be collected.

To evaluate the solute rejection of PES blend supports, 500 ppm solution of 10kDa PEG solution was used, whereas 1000 ppm NaCl solution was used as a feed solution for evaluating the solute rejection efficiency of TFC membranes. The rejection (R) of membranes was calculated according to Equation (2) as:

$$R(\%) = \left(1 - \frac{Cp}{Cf} \right) \times 100 \tag{2}$$

where Cf is the NaCl concentration in the feed solution, and Cp represents the NaCl concentration in the permeate. The concentration of NaCl in feed and permeate was calculated from the

conductivity values (µS/cm) measured using a Crison –EC Basic 30+ conductivity meter. Conductivity measurements were recorded at room temperature. The conductivity meter was calibrated using 0.01 M KCl solution with a conductivity of 1420 µS/cm prior to running the collected feed and permeate samples.

2.6 Antibacterial tests of TFC and TFN Membranes

Escherichia coli (E. coli) O157:H7 43895 was used to evaluate the antibacterial properties of TFC and TFN membranes. *E. coli* in 50 mL of Luria–Bertani (LB) broth was shaken at 200 rpm. The cells were harvested for 16 h and then separated from the LB broth by centrifugation. The supernatant was decanted and the pellets were re-suspended in phosphate buffered saline (PBS). The bacterial cells were then suspended in PBS to a cell density of approximately ×107 CFU/mL determined from optical density. *E. coli* suspensions were pipetted onto LB agar plates and spread over the surface. Membrane samples were placed in the middle of the agar plates and incubated at 37 ◦C for 24 h. After incubation, the agar plates were visually observed for the bacterial growth.

3.0 RESULTS AND DISCUSSIONS

3.1 Characterisation of CNT/PES and N-CNT/PES Supports

The first part of this study focuses on the discussion of physico-chemical and performance properties of CNT and N-CNT incorporated PES membrane supports. The loading of CNTs and N-CNTs within the PES polymer matrix was varied between 0.1 and 1.0 wt% to yield 0.1 wt% CNT/PES and 1.0 wt% CNT/PES, 0.1 wt% N-CNT/PES and 1.0 wt% N-CNT/PES membranes, respectively.

3.1.1 TEM Analysis of CNTs and N-CNTs

TEM images of CNTs and N-CNTs are shown in Figure 1. It can be seen that N-doping induced a change in morphology within the inner structure of the CNTs. In the case of CNTs, hollow-tubular structures can be observed while N-CNTs have the compartmentalised segments within the tubular structures resembling a typical bamboo morphology commonly found in N-CNTs [20, 21]. The presence of N atoms within the nanotube walls leads to the distortion of the hexagonal framework of graphene layers by creating curved pentagonal structures which leads to the formation of bamboo caps [22]. Additionally, N-doping leads to the formation of smaller tube diameters, i.e., the outer diameters for CNTs were in the range ∼34 – 52 nm while those of N-CNTs were between ∼ 31 – 42 nm, respectively. The decrease in diameters for N-CNTs can be associated with the interaction of the acid with the outermost graphene layers [23].

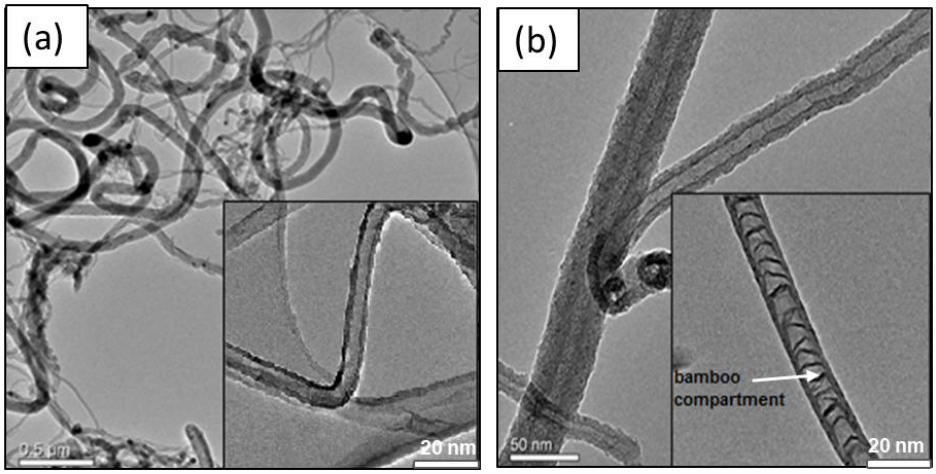

Figure 1 TEM images of (a) CNTs and (b) N-CNTs. Insets: TEM images of CNTs or N-CNTs recorded at higher magnifications

3.1.2. FT-IR Spectroscopic Analysis

The FT-IR spectroscopic analysis of PES and PES blend membranes was carried out in order to evaluate the surface chemistry of the membranes through functional group identification. All spectra show identical peaks at ~ 1590 - 1480 cm^{-1} (corresponding to C=C stretch of aromatic groups), at ~ 1309 - 1157 cm^{-1} (corresponding to S=O stretch vibration of the sulfone groups) and ~1231 cm^{-1} (corresponding to C-O-C stretches of the ether group); all peaks characteristic of PES backbone (Figure 2). However, the only noticeable difference in the spectra for PES blend membranes from that of bare PES, is the appearance of the peak at 1688 cm^{-1} due to C=O bonds of the carboxylic acid group. This is obviously due to the inclusion of acid-treated MWCNTs or N-CNTs into the PES polymeric matrix.

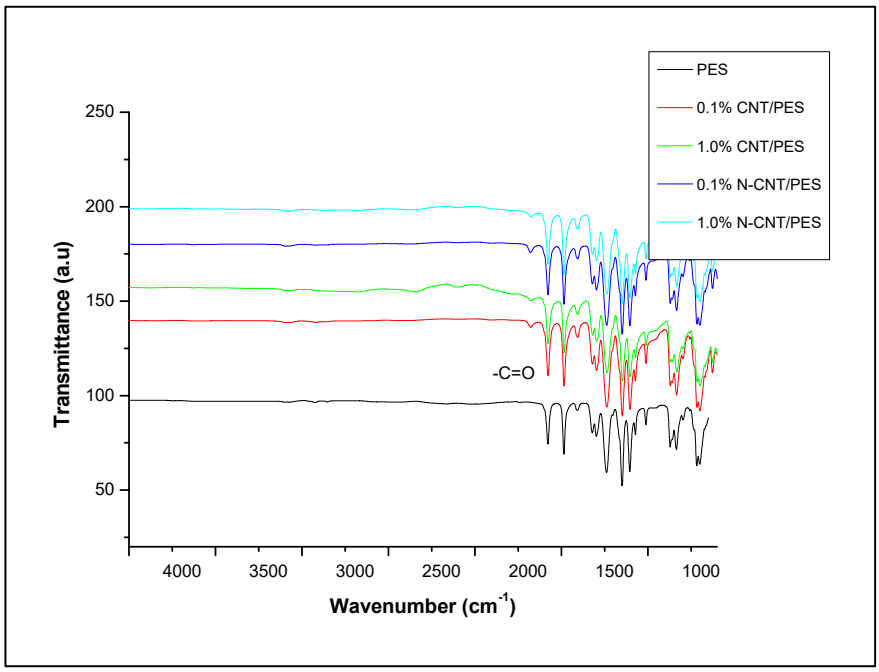

Figure 2 FT-IR spectra of bare PES and PES blend membranes

3.1.3 SEM Analysis of CNT/PES and N-CNT/PES Supports

In order to evaluate the influence of CNTs or N-CNTs on the PES membrane microstructure, SEM surface and cross-sectional analyses were conducted. The surface images in Figure 3 (a, c, e, g, i) depicts that the number of pores (porosity) and pore sizes increases after the inclusion of the of CNTs or N-CNTs onto the PES matrix. This can be associated with the enhanced and more facilitated phase separation process caused by the presence of hydrophilic additives CNTs or N-CNTs into the polymer matrix [24, 25]. The cross-sectional images of bare PES and PES blend membranes in Figure 3 (b, d, f, h, j) reveal that all membrane supports have a typical asymmetric structure; which comprises of a dense top layer and a porous sub-layer. Moreover, bare PES membranes (Figure 3 a) possesses very large finger-like structures in the porous sub-layer; the formation of which is facilitated by the fast exchange rate between the solvent and non-solvent during membrane formation. However, after the inclusion of 0.1 wt% CNTs and N-CNTs, the formation of finger-like microstructures in the membrane sublayer becomes less pronounced (Figure 3 d, h). The suppression of these finger-like microstructures becomes even more pronounced as the CNTs or N-CNTs loading is increased to 1.0 wt% (Figure 3 f, j), with tiny pores walls starting to develop (marked with X). Such an occurrence can be linked to an increase in viscosity of the casting solution upon increments in CNTs or N-CNTs loading. At high viscosities, the mixing-demixing rate between the solvent (NMP) and non-solvent (water) is hindered, thus resulting in a denser substructure with fewer finger-like structures and macrovoids. The presence of macrovoids tends to compromise the mechanical integrity of the membranes resulting in membrane rapture during high pressure application processes such as RO [26, 27]. As such, their absence is highly desired in the present study.

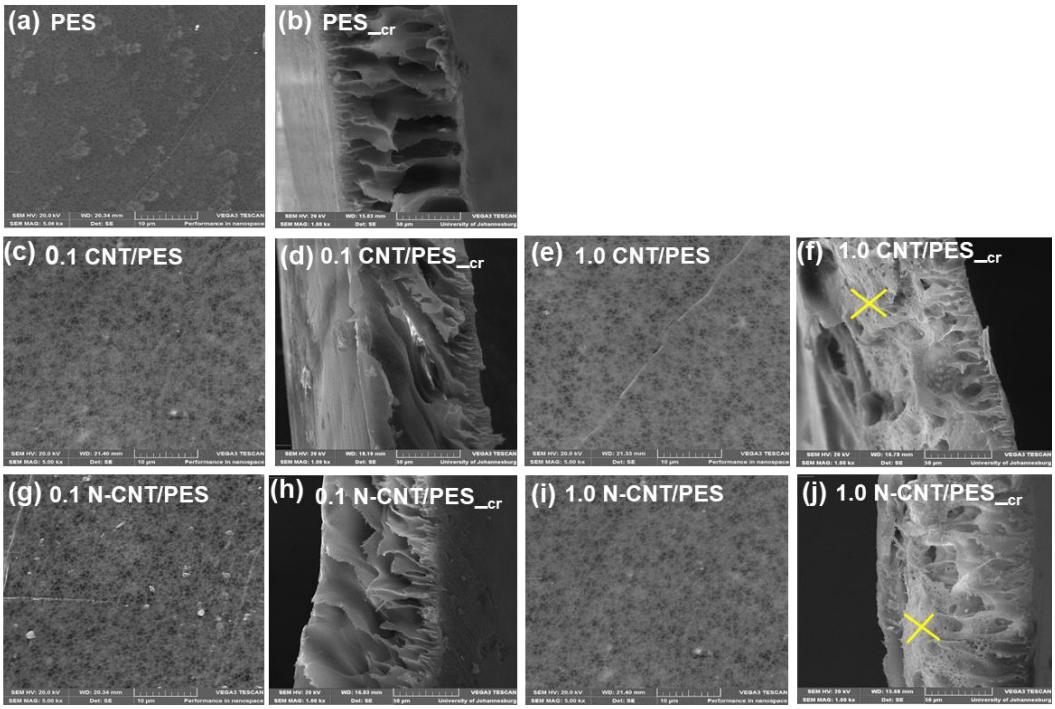

Figure 3 SEM surface (a, c, e, g, i) and cross-sectional images (b, d, f, h, j) of PES and PES blend membranes

3.1.4. Contact Angle Measurements and Water Uptake Studies

Table 2 presents the contact angle and water uptake values of PES and PES blended membranes. Generally, the measurement of contact angles for membranes gives an indication of the extent of hydrophilicity or hydrophobicity of the membrane surface [28]. It was found that the contact angle vales measured initially decreased from 66° for bare PES to 61° and 60° upon the inclusion of 0.1 wt.% of CNTs or N-CNTs into the PES matrix. The decrease in contact angle is indicative of improvements in the membrane surface hydrophilicity due to the inclusion of hydrophilic CNTs or N-CNT additives. These hydrophilic additives migrate spontaneously to the membrane/water interface during the phase inversion process to reduce the interfacial energy required thus rendering the membrane surface hydrophilic [29]. However, at 1.0 wt% of CNTs or N-CNT loading, no further enhancement in membrane surface hydrophilicity could be obtained, instead contact angles values increases. This could be due to irregular positioning and agglomeration of CNTs or N-CNTs within the membrane microstructure. Similar findings have been previously reported [18, 24].

Water uptake tests are crucial in determining the effectiveness of the prepared blended membranes as possible support layers for the manufacture of TFC membranes, i.e. the first step of interfacial polymerization involves the immersion of the support membrane in the aqueous diamine monomer solution. The values calculated from water uptake studies of PES blend membranes are shown in Table 3. It can be seen that the water uptake increases by 4.56% for 0.1 wt% CNT/PES and by 7.48% for 0.1 wt N-CNT/PES membranes from that of bare PES membrane. This can be correlated to the improvement in hydrophilicity of these blended membranes after the incorporation of CNTs or N-CNTs. The 0.1 wt% N-CNT/PES membranes had the lowest contact angle hence a higher water uptake. Nonetheless, water uptake decreased by 2.73% and 2.97% after the incorporation of 1.0 wt%. CNTs or N-CNTs. This observation can be associated with increase in solution viscosity and irregular collocation of nanoadditives on the polymeric matrices at higher loadings as was previously established from SEM cross-sectional images and from contact angles values of 1.0 wt% CNT/PES and 1.0 wt% N-CNT/PES membrane. Similar findings have been reported by Qiu *et al*. [30] and Vatanpour *et al*. [24].

Table 2 Water contact angles and water uptake tests of PES and PES blend supports

Membrane type	Porosity (%)	Contact angle (°)	Water uptake (%)	PEG Rejection (%)
PES	56	66.18 ± 0.05	38.92± 0.01	94.95± 0.21
0.1wt% CNT/PES	66	61.29 ± 0.27	43.48± 0.05	92.69± 0.14
0.1wt% N-CNT/PES	69	60.59 ± 0.05	46.40± 0.10	92.78± 0.11
1.0 wt% CNT/PES	64	70.66 ± 0.28	36.19± 0.04	94.04± 0.18
1.0 wt% N-CNT/PES	66	71.16 ± 0.89	35.95± 0.11	94.39± 0.15

3.1.5 Membrane Performance of CNT/PES and N-CNT/PES Supports

Figure 4 demonstrates that the pure water flux increases after the addition of 0.1 wt% CNTs or N-CNTs in the PES matrix but reduces as the nanoadditive loading is increased to 1.0 wt%. In the former, the increase in water permeation can be attributed to the increase in surface porosity and enhancement in membrane surface hydrophilicity of the 0.1% CNT/PES and 0.1 wt% N-CNT/PES membranes as elucidated from SEM and contact angle measurements. Apart from process operation conditions such as increases in applied transmembrane pressure, pure water flux membranes is controlled by surface hydrophilicity and membrane pore size [31]. In the latter, the decrease in water permeation can be ascribed to the to the formation of a denser substructure as a consequence of an increase in solution viscosity at higher CNTs or N-CNT loadings. The electrostatic interactions between the CNTs or N-CNTs at higher loadings causes them to form clusters within the PES polymer chains, leading to subtle reduction in hydrophilicity and membrane flux.

Although both CNT/PES and N-CNT/PES membranes show similar patterns in terms of pure water flux increases with the applied pressure, N-CNT/PES membranes exhibit slightly higher pure fluxes compared CNT/PES membranes. This observed behaviour can be linked to increase in surface reactivity of CNTs imparted by the presence of doped nitrogen atoms, which in turns enhances the compatibility between N-CNTs and PES matrix. The presence of hydrophilic functional groups on the CNTs and N-CNT surface accelerate the exchange rate between the solvent and non-solvent during phase inversion, leading to enhanced water permeation more particularly at low dosages. Further increments in CNT and N-CNT dosages causes the resultant PES blend membrane to adopt a similar permeation behaviour as that of a bare PES membrane. As such, the loading of CNTs or N-CNTs within the PES matrix should be kept low to achieve enhanced membrane performance.

In Table 2, the PEG 100kDa rejection of PES and PES blend membranes at 80 Psi. The measured rejections were 94.95%, 92.69%, 92.78%, 94.04% and 94.39% for PES, 0.1 wt% CNT/PES, 0.1wt% N-CNT/PES, 1.0 wt% CNT/PES and 1.0 wt% N-CNT/PES membranes respectively (see error bar graphs). The slight initial decline after the introduction of 0.1 wt.% of the CNTs or N-CNTs can be accounted for by the increase in surface porosity and pore sizes structure which was responsible for higher pure water fluxes, In this case the permeability-selectivity trade-off prevailed [32]. At 1.0 wt.% N-CNT loading, the formation of the dense sub-structure aided the increase in solute rejection.

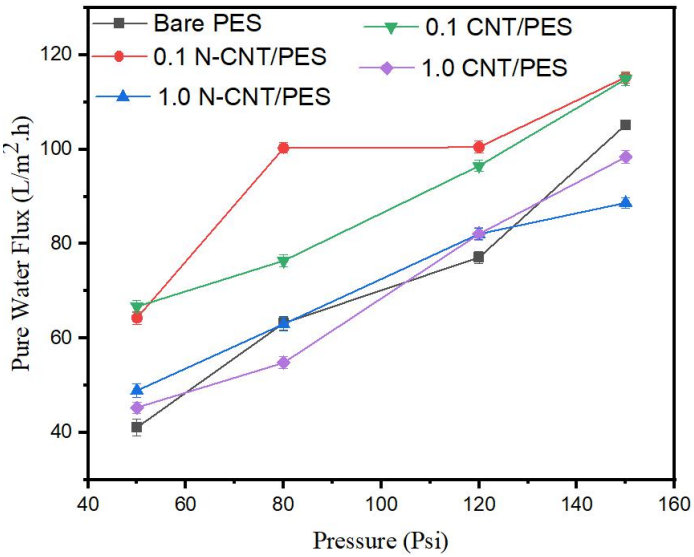

Figure 4 Pure water flux of PES and PES membrane blends as a function of pressure

3.1.6 Mechanical Strength Properties

Figure 5 shows the stress-strain of PES and PES blended membranes. The CNT incorporated PES membranes displayed much higher tensile strength at higher percentage elongation at both 0.1 wt.% and 1.0 wt.% loadings, compared to all PES membranes in the tested series. This was then followed by the N-CNT/PES membranes and bare PES membrane. The significant improvement in tensile strength of CNT incorporated PES membranes is attributable to the strong interaction between the PES and the CNTs via hydrogen bonding [15]. Although the cross-sectional morphologies of CNT/PES and N-CNT/PES membranes at 1.0 wt% loading are similar, in term of possession of a dense sub-layer structure, for the N-CNT incorporated PES, there were no significant or pronounced changes in tensile stress compared to bare PES membrane. This can be associated with the presence of the N atoms on the CNT backbone, which create interstitial spaces thus causing structural distortions in carbon nanotube framework. Nevertheless, the strain at break for N-CNT/PES was found to be slightly higher than that of bare PES membranes (from 22% to 27%) suggesting that the presence of the N-CNTs in the polymer matrix does contribute in part, by taking up some strain during the elongation process.

Due to the outstanding mechanical strength properties displayed by the 0.1 wt% CNT/PES support, combined with good membrane performance (high water permeability and solute rejection), all thin-film composite membranes discussed in this work, have been prepared on this support.

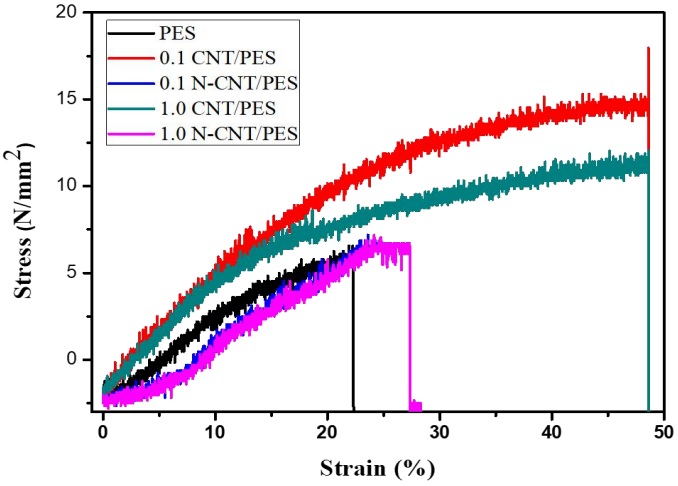

Figure 5 Stress-strain curves for different PES blended membranes

3.2 Characterisation of TFC and TFN Membranes

3.2.1 SEM Analysis

SEM surface images of TFC and TFN membranes shown in Figure 6 depict a "ridge and valley" morphology that is characteristic of the polyamide thin-film layer [33, 34]. There were no obvious visual differences in the surface images of TFC and TFN membranes (a, b) at SEM magnification of 25,000. However, when the magnification was increased to 50,000 x, small spherical particles were observed (indicated by white arrows) within the polyamide cross-linked network structure for the TFN membrane image Figure 6(d). The diameters of these particles (measured using Image J software) ranged from 30 to 40 nm. These particles are due to the attachment of nAg on the TFC surface. The energy dispersive spectroscopy (EDS) was used to confirm the presence of nAg in the membranes (Figure 7 b). The silver content in the TFN membrane was found to be 6.8 % from EDS analysis. Based on the EDS spectrum of TFC membrane (Figure 7 a), no silver could be detected. This suggests that the small grainy substances (marked in white circles) in the SEM image for TFC membrane at 50,000 x magnification (Figure 6 c) were due to the residual unreacted monomers on the membrane surface.

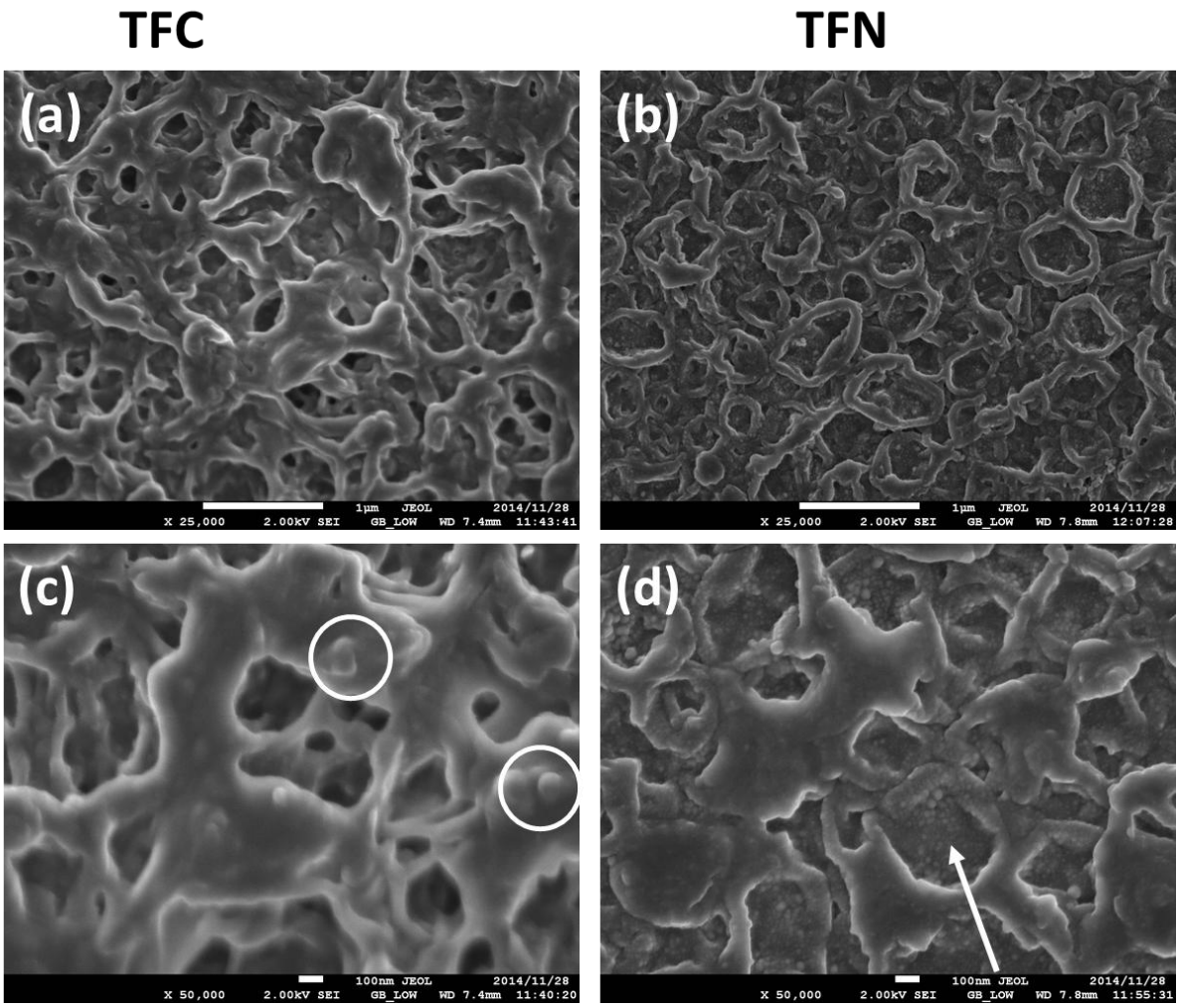

Figure 6 Surface SEM micrographs of (a,c) TFC and (b,d) TFN membranes at different magnifications (25,000 x and 50, 000 x)

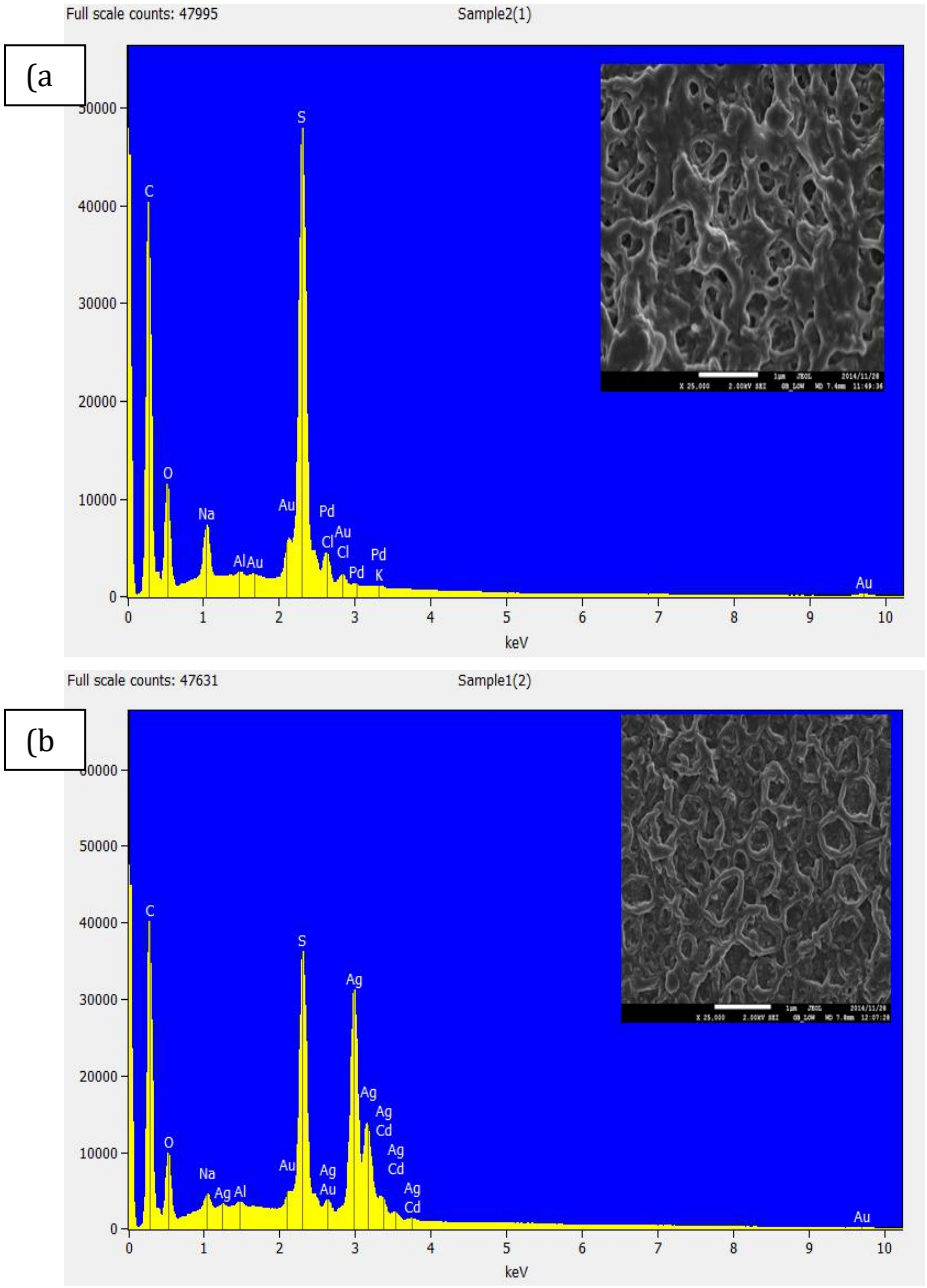

Figure 7 EDS spectra of (a) TFC membrane and (b) TFN membrane, showing the presence of Ag in the TFN membrane. Insert: SEM images of TFC and TFN membranes

3.2.2 AFM Analysis of TFC and TFN Membranes

The AFM images of TFC and TFN membranes are shown in Figure 8. Both membranes (TFC and TFN) showed nanoscale surface roughness (Table 3), which is another characteristic feature of polyamide TFC membranes prepared by interfacial polymerisation method (Hoek, *et al*., 2001). The root mean square surface roughness (Rq) of the TFN membrane of 52.43 is slightly decreased from that of bare TFC of 59.57nm. The decrease in surface roughness of the TFN membrane can be attributed to uniform dispersion of the nAg particles on the membrane surface, which also led to the improvement in surface hydrophilicity. The membrane surface

roughness obtained is comparable to what has been reported previously by other researchers [14, 33]. Minimal membrane surface roughness is a desirable property in RO seawater membranes to reduce the membranes' propensity to fouling because of the reduced adsorption sites for foulant attachment [4].

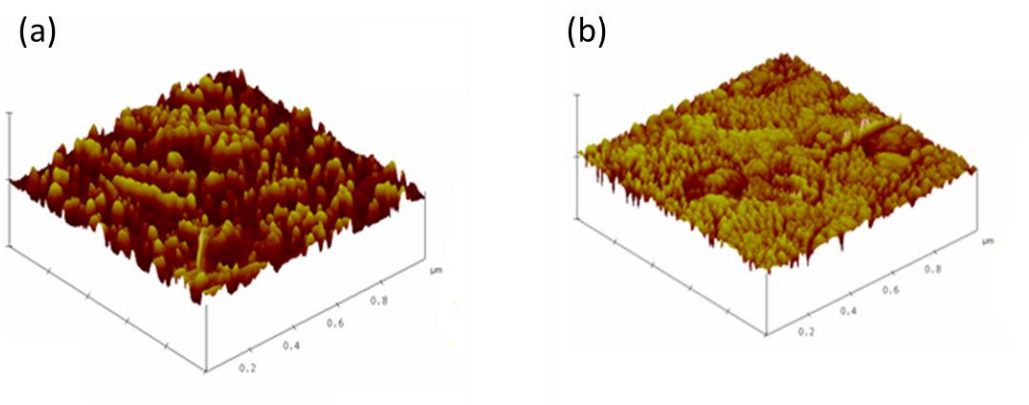

Figure 8 (AFM images of (a) TFC and (b) TFN membranes

3.2.3 Contact Angle Measurements of TFC and TFN Membranes

In Table 3, contact angle measurements of TFC and TFN membranes are reported. A decrease in contact angle from 70.23º for TFC membrane to 59.91º for TFN membrane can be observed. This remarkable decrease suggests that the added nAg improves the membrane surface hydrophilicity. Liu and Hurt [35] predicted the mechanism of hydrophilicity improvement to be due to the release of Ag+ ions in the aqueous phase and the subsequent adsorption of the ions on the nAg surface during the formation of the hydrated Ag+ ion. This is the probable source of the nAg hydrophilicity. Zodrow *et al*., [3] also reported that an increase in the nAg content in the membrane results to an improvement in membrane hydrophilicity.

Table 3 Surface roughness parameters and water contact angles of TFC and TFN membranes

Membrane	Roughness parameter Rq(nm)	Ra(nm)	Contact angle (°)
TFC	59.57± 1.5	48.27± 0.8	70.23± 0.1
TFN	52.43± 1.3	42.23± 1.0	59.91± 0.5

Rq= room mean square roughness; Ra= average roughness

3.2.4 XRD and FT-IR Spectroscopic Analysis

Surface crystallization of TFC and TFN membranes was studied by using XRD spectroscopy analysis. The XRD pattern of the TFN membrane (Figure 9 (a)) shows four new diffraction peaks corresponding to Ag between 2θ of 37º, 44º, 64º and 77º; assigned to Ag (111),

Ag (200), Ag (220) and Ag (311) respectively. These peaks were absent in the XRD pattern of bare TFC membrane. The emergence of the assigned peaks supports the evidence already established from EDS analysis of the TFN membranes that, indeed nAg were attached on the TFN membrane surface.

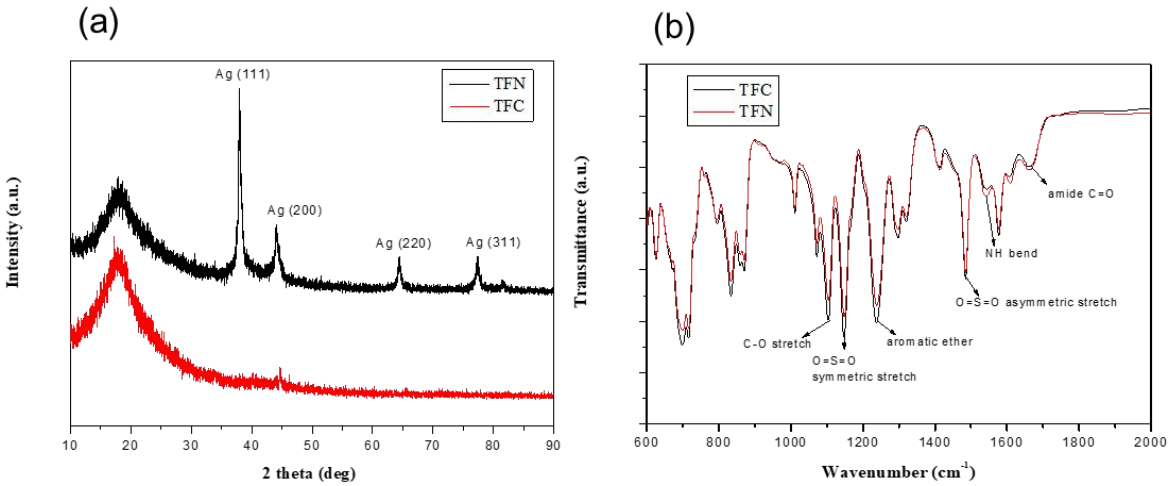

Figure 9 (a) XRD spectra and (b) FT-IR spectra of TFC and TFN membranes

FT-IR spectra of TFC and TFN membranes are shown in Figure 9 (b). The two spectra completely overlap and both show intense peaks at 1104 cm^{-1} (-CO stretch), 1147 cm^{-1} (O=S=O symmetric stretch), 1235 cm^{-1} (aromatic ether), 1488 cm^{-1} (O=S=O asymmetric stretch), 1536 cm^{-1} (-NH bend) and 1663 cm^{-1} (amide -C=O). The completely identical FT-IR spectra of TFC and TFN membrane indicate that the NaBH4 solution did not reduce the –C=O and -NH groups on the polyamide layer; these chemical group functionalities are the main constituents of the polyamide backbone.

3.2.5 Thermogravimetric Analysis TFC and TFN Membranes

In Figure 10, the mass loss between 100 – 200 ◦C in the TGA curves of TFC and TFN membranes corresponds to loss of residual solvent after the fabrication of the membrane The thermal degradation temperature of 454 ◦C for the TFN membrane is lower than that of the TFC membrane (500 °C) suggesting that its thermal stability has been reduced. Further, only 94% of the TFN membrane sample undergoes thermal degradation, leaving a residual mass of 6% which is nAg residue. On the other hand, the TFC membrane undergoes almost complete thermal degradation with a residual mass of 0.07%. The CNT content within the TFC support is very low, degradation due to the presence of CNTs is negligible. The decrease in thermal stability of the TFN membrane can be associated with the presence of nAg in the polyamide layer membrane surface. The presence of silver induces structural distortions in the polyamide layer of the membrane due to the interaction between nAg and the polyamide layer thus resulting in a decrease in thermal stability. From the EDS analysis of TFN membrane, the Ag content was found to be 6.8% - this resembles the residual weight percentage of the TFN membrane from the TGA plot. The residual contents of the TFN membrane may be predominantly composed of nAg particles.

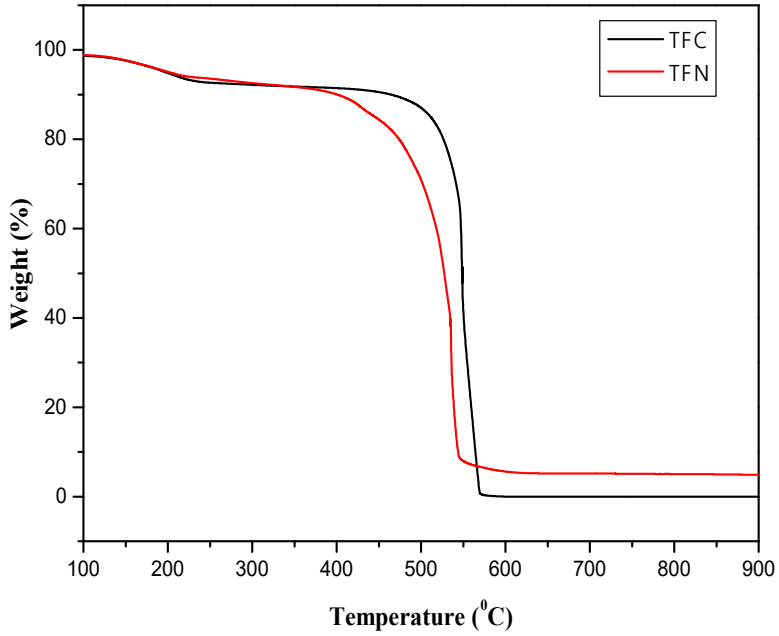

Figure 10 TGA plots of TFC and TFN membranes

3.2.6 Evaluation TFC and TFN Membrane Performance

Pure water flux of the TFC and TFN membranes was evaluated as a function of applied pressure (Figure 11). In both membranes, pure water flux increased linearly with the applied pressure i.e. the higher the applied pressure, the lower the membranes hydraulic resistance to flow, resulting in more water being forced through the membrane. Pure water flux increased from 4.88 L/m^2.h for the TFN membrane at 100 Psi to 35.85 L/m^2.h at 300 Psi. Moreover, pure water flux for TFN membrane was found to be higher than that of the TFC membrane. For example, at 150 Psi, the pure water flux for TFC membrane was found to be 16.74 L/m^2.h while that of TFN membranes was 22.86 L/m^2.h. This improvement in pure water flux can be ascribed to the enhanced hydrophilicity of the TFN membrane which is caused by the presence on nAg on the membrane surface. At higher membrane surface hydrophilicities, more water molecules are attracted towards the membrane surface, fostering more interactions with the membrane surface, resulting in higher membrane permeability upon the application of pressure. Additionally, the presence of granular substances on the TFC RO membrane surface as a result of residual unreacted monomers, as established from SEM analysis, could also impart on the lower water permeability of the TFC membrane, while uniform dispersion on nAg on TFN membrane surface, which resulted in formation of formation of smoother membrane surface, aided the observed increased water permeability.

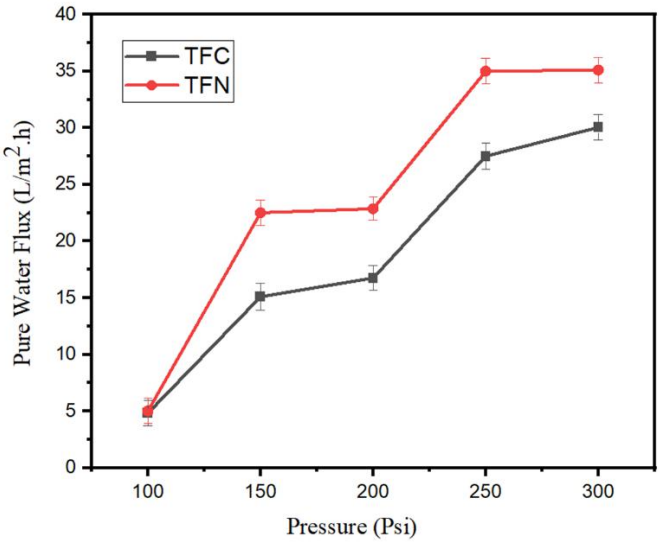

Figure 11 Pure water flux against pressure of TFC and TFN membranes

The NaCl solute rejection of the TFC membrane was found to be 98.38% while that of TFN membranes was 99.40%. This means that the rejection of the TFN membranes only increased by 1.02% from that of bare TFC membrane. These results are similar to those reported by Kim *et al*., (2012) in which the presence of nAg in the polyamide layer and N-CNTs in the support layer significantly improved the TFN membranes' permeability with minimal impact on the solute rejection capacity of the membrane [14].

3.2.7 Antibacterial Performance of TFC and TFN Membranes

The antibacterial tests conducted on the TFC and TFN membranes upon contact with *E. coli* bacterial suspension can be observed in Figure 12. An immense bacterial adhesion can be observed around the culture containing TFC membranes, whereas a clear zone of inhibition in the areas surrounding the TFN membranes can be seen in Figure 13(b). Moreover, there were no bacterial colonies formed in the culture plate containing TFN membranes. The observed results are attributable to the biocidal effects imparted by the nAg present on the surface of the TFN membrane. Due to the location of nAg on the TFN membrane surface, it can be concluded that the bacteria were destroyed upon direct contact with nAg enriched TFN membranes [34]. The antibacterial behaviour displayed by the fabricated TFN membranes is beneficial in minimising the growth of bacteria, thus combating membrane biofouling.

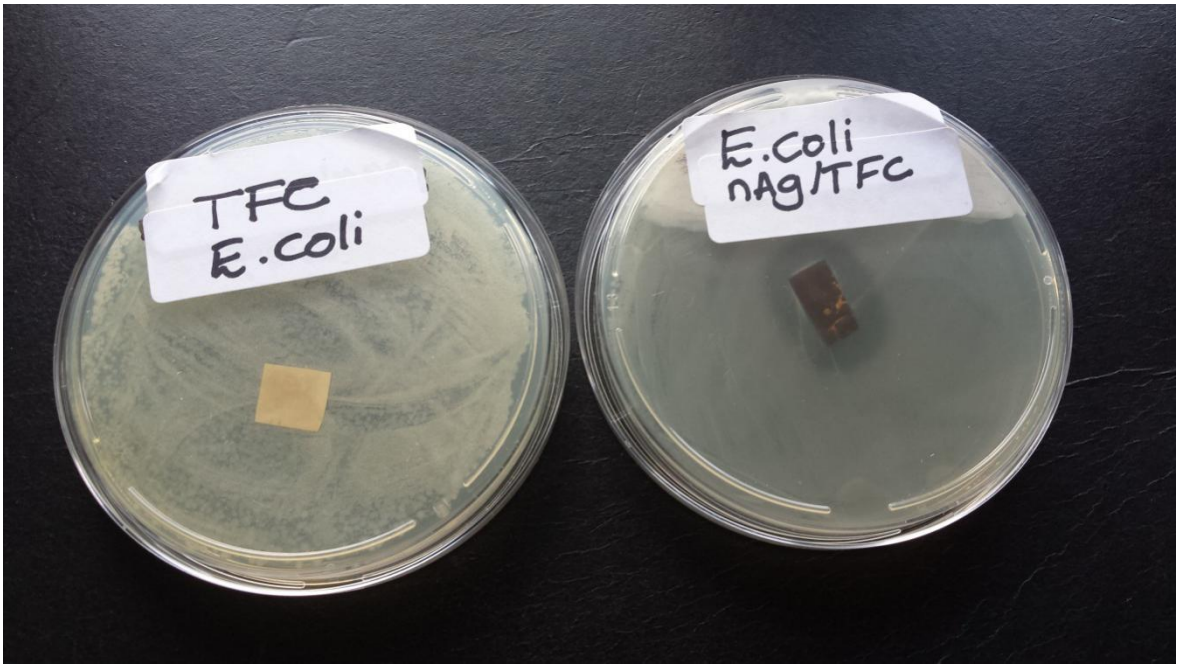

Figure 12 Antibacterial effect on *E.coli* of (a) TFC and (b) TFN membranes observed in disk diffusion test

4.0 CONCLUSION

TFC and TFN membranes were successfully synthesized by the interfacial polymerisation method over PES supports containing oxidised multi-walled CNTs. A comparability study on the physico-chemical and performance properties of CNT/PES and N-CNT/PES supports proved that the CNT/PES supports display far better outstanding mechanical strength properties with comparable pure water flux and solute (PEG 10kDa) rejection with N-CNT/PES supports. As such, the inclusion of low dosages oxidised multi-walled CNTs onto PES matrices is a far more plausible approach in the preparation of high performance and high mechanical strength supports for TFC membranes. Additionally, in-situ generated nanosilver were successfully formed and immobilised on the surface of a polyamide layer of the TFC membrane by an in-situ chemical reduction reaction to form TFN membrane. The TFN membrane surface properties such as hydrophilicity and roughness were greatly improved due to the presence of nAg on the polyamide layer. Pure water flux of the TFN membrane was enhanced without compromising the NaCl rejection efficiency of the TFN membrane. Furthermore, TFN membranes fabricated showed good antibacterial properties against the growth of *E. coli* as evidence by the absence of bacterial colonies formed on the culture plate. The study conducted provided more insights on modification of TFC membrane supports using carbon-based nanomaterial additives. Moreover, the nanosilver modified TFN membranes prepared displayed promising features for application in the desalination of brackish waters.

ACKNOWLEDGMENTS

The authors wish to acknowledge the University of Johannesburg and the University of South Africa, for

providing facilities to conduct this work and for financial support.

REFERENCES

[1] B. H. Jeong, E. M. Hoek, Y. Yan, A. Subramani, X. Huang, G. Hurwitz, A. Ghosh, A. Jawor. 2007. Interfacial Polymerization of Thin Film Nanocomposites: A New Concept for Reverse Osmosis Membranes. *J. Membr. Sci.* 294(1-2): 1-7.

[2] M. F. Goosen, S. Sablani, R. Roque-Malherbe. 2008. Membrane Fouling: Recent Strategies and Methodologies for Its Minimization. Handbook of Membrane Separations: Chemical, Pharmaceuticals, Food and Biotechnological Applications CRC Press. Taylor and Francis. 325-41.

[3] K. R. Zodrow, M. E. Tousley, M. Elimelech. 2014. Mitigating Biofouling on Thin-film Composite Polyamide Membranes using a Controlled-release Platform. *J. Membr. Sci.* 453: 84-91.

[4] N. Misdan, W. J. Lau, A. Ismail. 2012. Seawater Reverse Osmosis (SWRO) Desalination by Thin-film Composite Membrane—Current Development, Challenges and Future Prospects. *Desalination*. 287: 228-37.

[5] C. Marambio-Jones, E. M. V. Hoek. 2010. A Review of the Antibacterial Effects of Silver Nanomaterials and Potential Implications for Human Health and the Environment. *J. Nanopart. Res.* 12(5): 1531-51.

[6] M. Ben-Sasson, X. Lu, E. Bar-Zeev, K.R. Zodrow, S. Nejati, G. Qi, E.P. Gainnelis, M. Elimelech. 2014. In Situ Formation of Silver Nanoparticles on Thin-film Composite Reverse Osmosis Membranes for Biofouling Mitigation. *Water Res.* 62: 260-70.

[7] K. Zodrow, L. Brunet, S. Mahendra, D. Li, A. Zhang, Q. Li, P. J. J. Alvarez. 2009. Polysulfone Ultrafiltration Membranes Impregnated with Silver Nanoparticles Show Improved Biofouling Resistance and Virus Removal. *Water Res.* 43(3): 715-23.

[8] I. Sawada, R. Fachrul, T. Ito, Y. Ohmukai, T. Maruyama, H. Matsuyama. 2012. Development of a Hydrophilic Polymer Membrane Containing Silver Nanoparticles with Both Organic Antifouling and Antibacterial Properties. *J. Membr. Sci.* 387: 1-6.

[9] D.Y. Koseoglu-Imer, B. Kose, M. Altinbas, I. Koyuncu. 2013. The Production of Polysulfone (PS) Membrane with Silver Nanoparticles (AgNP): Physical Properties, Filtration Performances, and Biofouling Resistances of Membranes. *J. Membr. Sci*. 428: 620-8.

[10] J. S. Taurozzi, H. Arul, V. Z. Bosak, A. F. Burban, T. C. Voice, M. L. Bruening, V. V. Tarabara. 2008. Effect of Filler Incorporation Route on the Properties of Polysulfone–Silver Nanocomposite Membranes of Different Porosities. *J. Membr. Sci.* 325(1): 58-68.

[11] X. Cao, M. Tang, F. Liu, Y. Nie, C. Zhao. 2010. Immobilization of Silver Nanoparticles Onto Sulfonated Polyethersulfone Membranes as Antibacterial Materials. *Colloids Surf. B.* 81(2):555-62.

[12] E.M. Hoek, S. Bhattacharjee, M. Elimelech. 2003. Effect of Membrane Surface Roughness

on Colloid− Membrane Dlvo Interactions. *Langmuir.* 19(11): 4836-47.

[13] M. Sile-Yuksel, B. Tas, D.Y. Koseoglu-Imer, I. Koyuncu. 2014. Effect of Silver Nanoparticle (AgNP) Location In Nanocomposite Membrane Matrix Fabricated with Different Polymer Type on Antibacterial Mechanism. *Desalination.* 347: 120-30.

[14] E. S Kim, G. Hwang, M. G El-Din, Y. Liu. 2012. Development of Nanosilver and Multi-Walled Carbon Nanotubes Thin-Film Nanocomposite Membrane for Enhanced Water Treatment. *J. Membr. Sci.* 394: 37-48.

[15] N. Phao, E. N. Nxumalo, B. B. Mamba, S. D. Mhlanga. 2013. A Nitrogen-Doped Carbon Nanotube Enhanced Polyethersulfone Membrane System for Water Treatment. *Phys. Chem. Earth., Parts A/B/C*. 66:148-56.

[16] S. Y. Lee, H. J. Kim, R. Patel, S. J. Im, J. H. Kim, B. R. Min. 2007. Silver Nanoparticles Immobilized on Thin Film Composite Polyamide Membrane: Characterization, Nanofiltration, Antifouling Properties. *Polym. Adv. Technol.* 18(7): 562-8.

[17] H. L. Yang, J. Chun-Te Lin, C. Huang. 2009. Application of Nanosilver Surface Modification to RO Membrane and Spacer for Mitigating Biofouling in Seawater Desalination. *Water Res.* 43(15): 3777-86.

[18] N. N. Gumbi, M. Hu, B. B. Mamba, J. Li, E. N. Nxumalo. 2018. Macrovoid-free PES/SPSf/O-MWCNT Ultrafiltration Membranes with Improved Mechanical Strength, Antifouling and Antibacterial Properties. *J. Membr. Sci.* 566: 288-300.

[19] N. N. Gumbi, J. Li, B. B. Mamba, E. N. Nxumalo. 2020. Relating the Performance of Sulfonated Thin-Film Composite Nanofiltration Membranes to Structural Properties of Macrovoid-Free Polyethersulfone/Sulfonated Polysulfone/O-MWCNT Supports. *Desalination.* 474: 114176.

[20] E. N. Nxumalo, V. O. Nyamori, N. J. Coville. 2008. CVD Synthesis of Nitrogen Doped Carbon Nanotubes Using Ferrocene/Aniline Mixtures. *J. Organomet. Chem.* 693(17): 2942-8.

[21] X. Li, G. Zhu, Z. Xu. 2012. Nitrogen-doped Carbon Nanotube Arrays Grown on Graphene Substrate. *Thin Solid Films*. 520(6): 1959-64.

[22] B. G. Sumpter, V. Meunier, J. M. Romo-Herrera, E. Cruz-Silva, D. A. Cullen, H. Terrones, D. J. Smith, M. Terrones. 2007. Nitrogen-mediated Carbon Nanotube Growth: Diameter Reduction, Metallicity, Bundle Dispersability, and Bamboo-Like Structure Formation. *ACS Nano.* 1(4): 369-75.

[23] M. A. Motchelaho, H. Xiong, M. Moyo, L. L. Jewell, N. J. Coville. 2011. Effect of Acid Treatment on the Surface of Multiwalled Carbon Nanotubes Prepared from Fe–Co Supported on CaCO3: Correlation with Fischer–Tropsch Catalyst Activity. *J. Mol. Catal. A. Chem.* 335(1-2): 189-98.

[24] V. Vatanpour, S.S. Madaeni, R. Moradian, S. Zinadini, B. Astinchap. 2011. Fabrication and Characterization of Novel Antifouling Nanofiltration

Membrane Prepared from Oxidized Multiwalled Carbon Nanotube/Polyethersulfone Nanocomposite. *J. Membr. Sci*. 375(1-2): 284-94.

[25] A. Rahimpour, M. Jahanshahi, S. Khalili, A. Mollahosseini, A. Zirepour, B. Rajaeian. 2012. Novel Functionalized Carbon Nanotubes for Improving the Surface Properties and Performance of Polyethersulfone (PES) Membrane. *Desalination*. 286: 99-107.

[26] D. M. Wang, F. C Lin, T. T, W. J. Lau. 1998. Formation Mechanism of the Macrovoids Induced by Surfactant Additives. *J. Membr. Sci.* 142(2): 191-204.

[27] H. Ogawa, T. Kanaya, K. Nishida, G. Matsuba. 2008. Phase Separation and Dewetting in Polystyrene/poly (vinyl methyl ether) Blend Thin Films in a Wide Thickness Range. *Polymer.* 49(1): 254-62.

[28] E. Celik, H. Park, H. Choi, H. Choi. 2011. Carbon Nanotube Blended Polyethersulfone Membranes for Fouling Control in Water Treatment. *Water Res.* 45(1): 274-82.

[29] M. Sun, Y. Su, C. Mu, Z. Jiang. 2010. Improved Antifouling Property of PES Ultrafiltration Membranes using Additive of silica− PVP Nanocomposite. *Ind. Eng. Chem. Res*. 49(2): 790-6.

[30] S. Qiu, L. Wu, X. Pan, L. Zhang, H. Chen, C. Gao. 2009. Preparation and Properties of Functionalized Carbon Nanotube/PSF Blend Ultrafiltration Membranes. *J. Membr. Sci.* 42(1-2): 165-72.

[31] P. Daraei, S. S. Madaeni, N. Ghaemi, M. A. Khadivi, B. Astinchap, R. Moradian. 2013. Enhancing Antifouling Capability of PES Membrane via Mixing with Various Types of Polymer Modified Multi-Walled Carbon Nanotube. *J. Membr. Sci.* 444: 184-91.

[32] G. R. Xu, J. N. Wang, C. J. Li. 2013. Strategies for Improving the Performance of the Polyamide Thin Film Composite (PA-TFC) Reverse Osmosis (RO) Membranes: Surface Modifications and Nanoparticles Incorporations. *Desalination.* 328: 83-100.

[33] E. M. V. Hoek, S. Hong, M. Elimelech. 2001. Influence of Membrane Surface Properties on Initial Rate of Colloidal Fouling of Reverse Osmosis and Nanofiltration Membranes. *J. Membr. Sci*. 188(1): 115-28.

[34] Yin, J., Yang, Y., Z. Hu, B. Deng. 2013. Attachment of Silver Nanoparticles (AgNPs) onto Thin-Film Composite (TFC) Membranes through Covalent Bonding to Reduce Membrane Biofouling. *J. Membr. Sci*. 441: 73-82.

[35] J. Liu, R. H. Hurt. 2010. Ion Release Kinetics and Particle Persistence in Aqueous Nano-Silver Colloids. Environ. *Sci. Technol.* 44(6): 2169-75.